Electronic Supplementary Material (ESI) for Sustainable Energy & Fuels.

Supporting Information

Tuning Defects in the MoS_2/Reduced Graphene Oxide 2D Hybrid Materials for Optimizing Battery Performance

Kamalambika Muthukumar, Levon Leban II, Archana Sekar, Ayyappan Elangovan, Nandini Sarkar, and Jun Li*

Department of Chemistry, Kansas State University, Manhattan, Kansas, 66506, USA.

Figure S1. The full scale and expanded region of Raman spectra of (a, b) MoS_2/rGO-325, (c, d) MoS_2/rGO-250 and (e, f) MoS_3/rGO intermediate product.

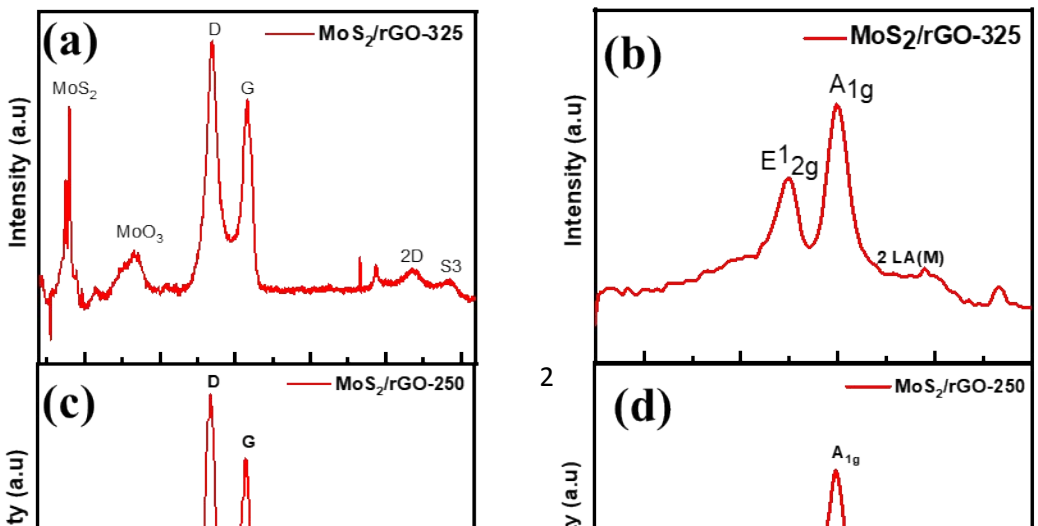

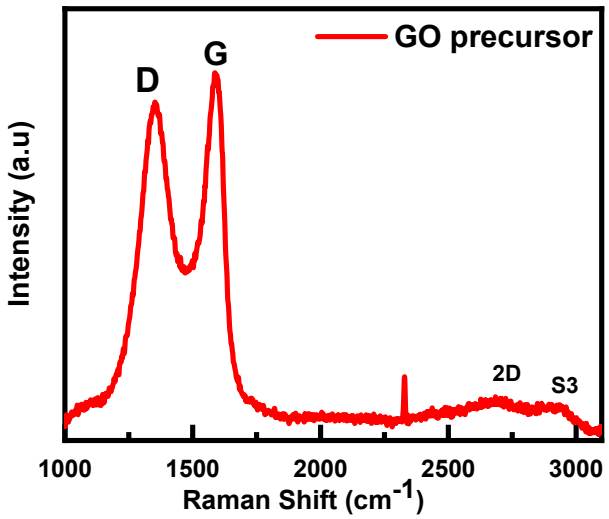

Figure S2. Raman Spectra of graphene oxide (GO) precursor material.

Figure S1. The full scale and expanded region of Raman Spectra of (a, b) MoS_2/rGO-600, (c, d) MoS_2/rGO-325 and (e, f) MoS_3/rGO intermediate product.

Table S1. Raman Analysis of GO precursor and MoS_2/rGO hybrids

Sample	**I_D/I_G**	**I_{S3}/I_{2D}**
GO Precursor	0.9	1.7
MoS_3/rGO-intermediate	1.3	0.3
MoS_2/rGO-250	1.3	0.3
MoS_2/rGO-325	1.3	0.4
MoS_2/rGO-600	1.3	0.4

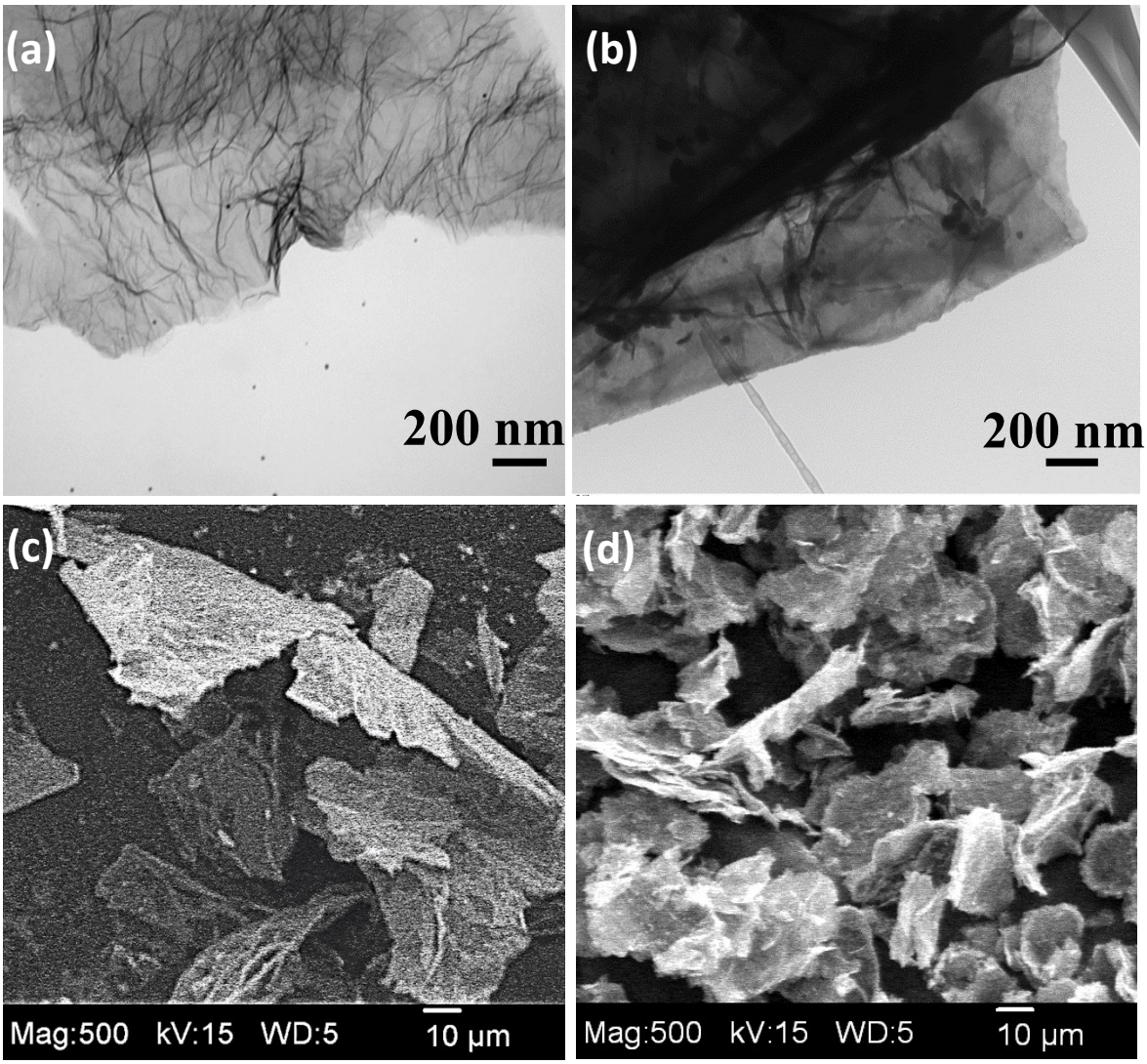

Figure S3. TEM images of (a) bare rGO nanosheets and (b) the MoS_3/rGO intermediate. (c) and (d): SEM images of these two samples, respectively. The bare rGO sample was prepared with microwave irradiation in absence of ATM precursors before subjected to thermal annealing at 600 °C in 3% H_2 and 97% Ar. The MoS_3/rGO intermediate was obtained after the microwave irradiation in presence of ATM precursors but was not subjected to the thermal annealing.

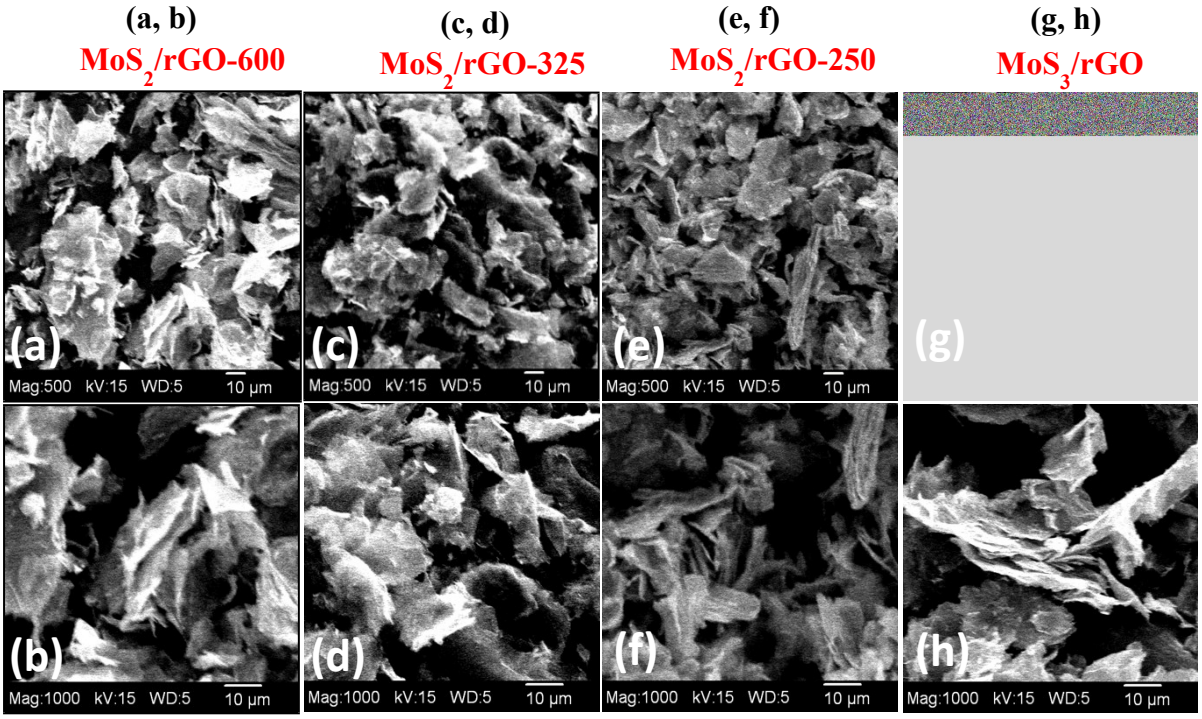

Figure S4. Low- and higher-magnification FESEM images of (a, b) MoS_2/rGO-600, (c, d) MoS_2/rGO-325, (e, f) MoS_2/rGO-250, and (g, h) MoS_3/rGO-intermediate.

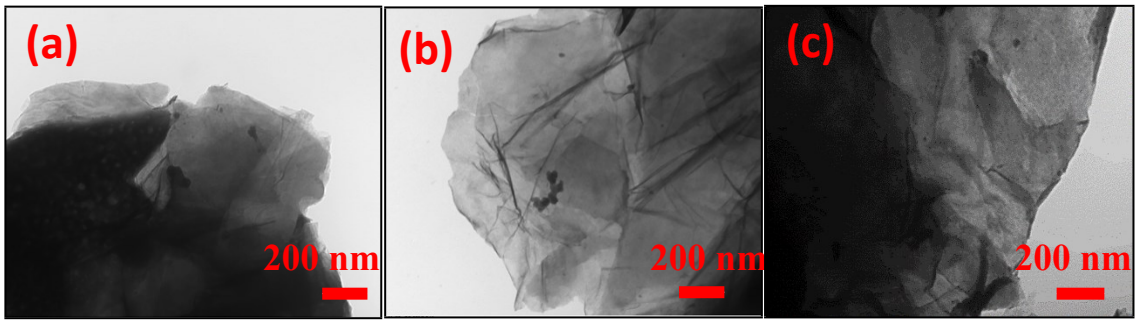

Figure S5. TEM images of (a) MoS_2/rGO-250, (b) MoS_2/rGO-325, and (c) MoS_2/rGO-600.

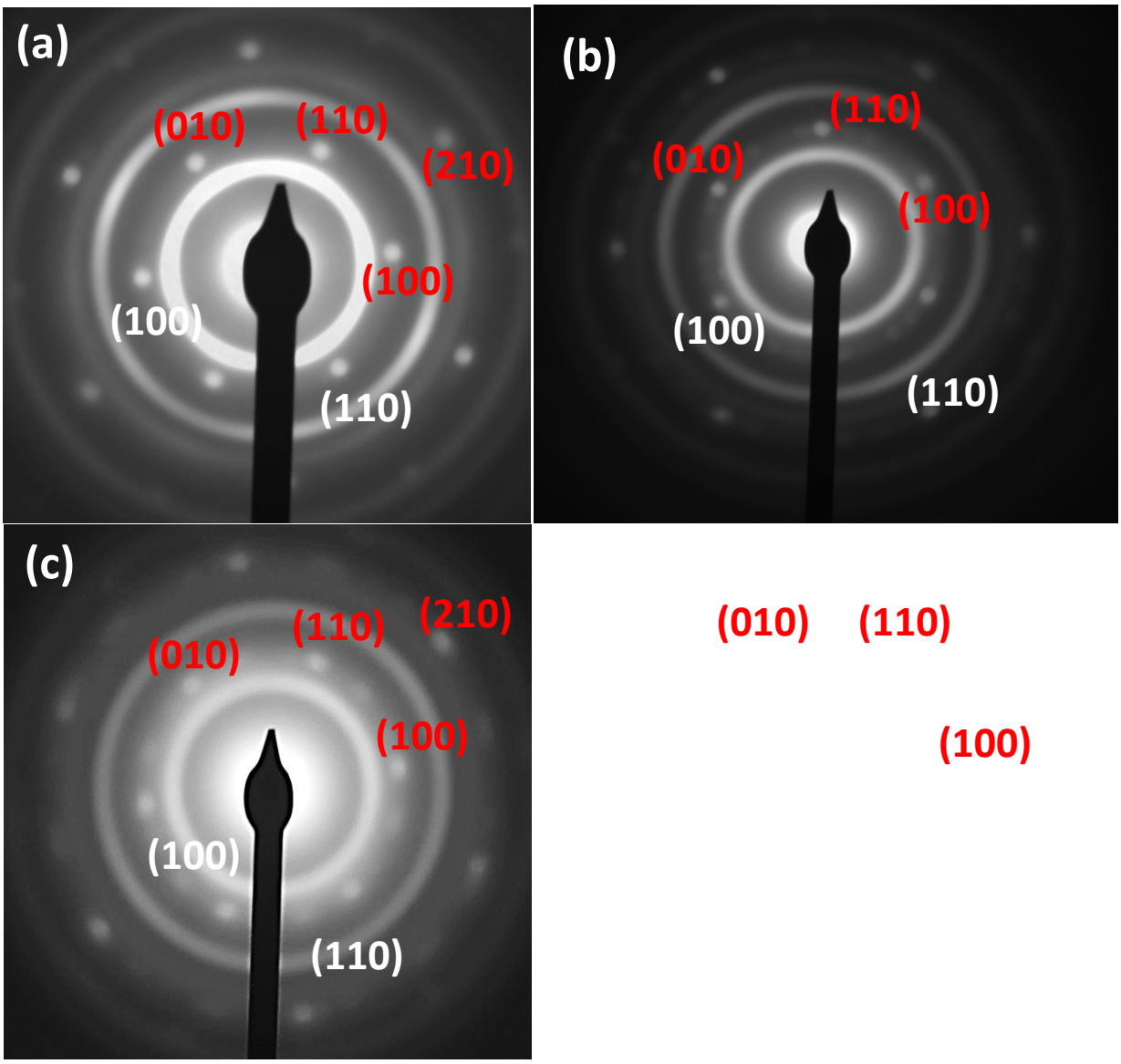

Figure S6. SAED patterns of (a) MoS_2/rGO-600, (b) MoS_2/rGO-325, (c) MoS_2/rGO-250, and (d) MoS_3/rGO intermediate. The red-colored indices at the top indicate the isolated 2D electron diffraction spots with the six-fold symmetry from the rGO nanosheets, while the white indices at the bottom indicate the continuous rings of 2D powder electron diffraction from MoS_2 nanopatches with random rotational orientations in the rGO plane.

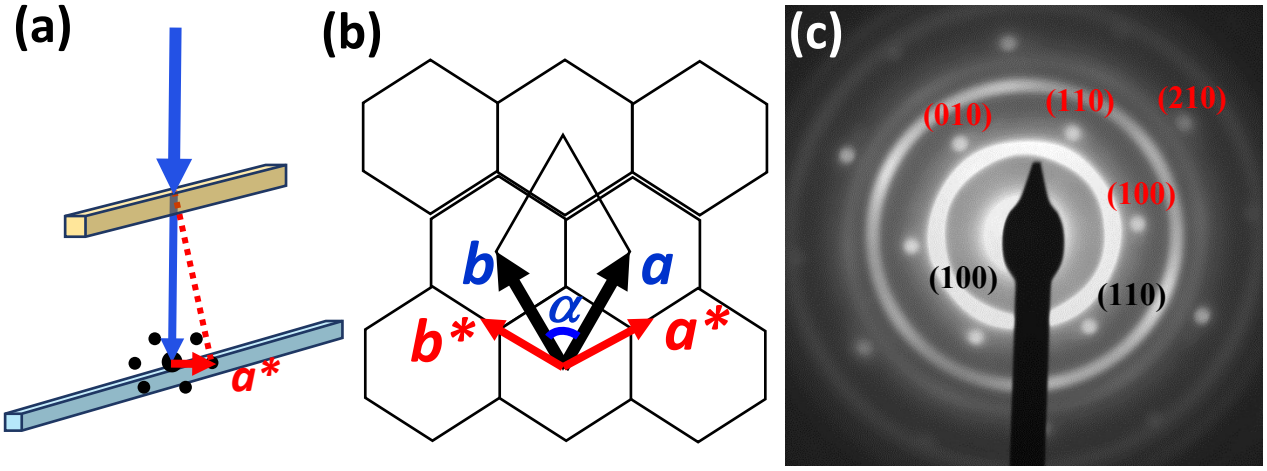

(d)

- **For 2D crystals with a hexagonal lattice:**
  a = b, a = 60°

  a - real space lattice; ***a**** - reciprocal space lattice

  $\boldsymbol{a \cdot a^* = 2\pi}$ i.e. a x a* x cos30° = 2 **π**

  a* = 2 **π** /(a×cos30°) or a = 2 **π** /(a*×cos30°)

- **For isolated SAED spots from rGO:**
  rGO: a = 2.46 Å => a* = 2.948 $Å^{-1}$

- **Use a* of rGO to calibrate the *a** of the continuous rings from MoS_2:**

  (100) ring of MoS_2: a*= 2.29 $Å^{-1}$ => a = 3.17 Å

Figure S7. (a) Schematic illustration of the SAED with the electron beam perpendicular to the 2D crystal plane. (b) The relationship of the real space 2D hexagonal lattice ***a*** and ***b*** and the reciprocal diffraction lattice (***a**** and ***b****). (c) The SAED pattern of MoS_2/rGO-600. (d) The procedure to derive the MoS_2 lattice in reference to the sharp hexagonal SAED pattern of the 2D monocrystalline rGO nanosheets.

Table S2. The parameters derived from deconvolution of Mo 3d and S 2p XPS spectra.

		MoS_3/rGO intermediate		MoS_2/rGO-250		MoS_2/rGO-325		MoS_2/rGO-600	
		B.E. (eV)	**Atomic % in the same element**	**B.E. (eV)**	**Atomic % in the same element**	**B.E. (eV)**	**Atomic % in the same element**	**B.E. (eV)**	**Atomic % in the same element**
Mo^{4+}	**$3d_{5/2}$**	229.08	28.58	229.03	83.08	229.12	66.41	229.28	68.24
	$3d_{3/2}$	232.21		232.16		232.25		232.41	
Mo^{5+}	**$3d_{5/2}$**	229.32	19.39	230.52	9.44	Mo $^{5+}$ is not present in this sample		Mo $^{5+}$ is not present in this sample	
	$3d_{3/2}$	232.45		233.65					
Mo^{6+}	**$3d_{5/2}$**	232.11	52.03	232.68	7.48	231.90	33.58	232.18	31.75
	$3d_{3/2}$	235.24		235.81		235.03		235.31	
S^{2-}	**$2p_{3/2}$**	162.59	45.99	161.68	46.46	161.93	86.50	162.09	100
	$2p_{1/2}$	163.78		162.47		163.21		163.27	
S_2^{2-}	**$2p_{3/2}$**	164.76	54.01	162.94	53.54	163.41	13.50		
	$2p_{1/2}$	165.79		164.10		164.58			
Mo : S		1:2.4		1:2.9		1:2.3		1:1.9	

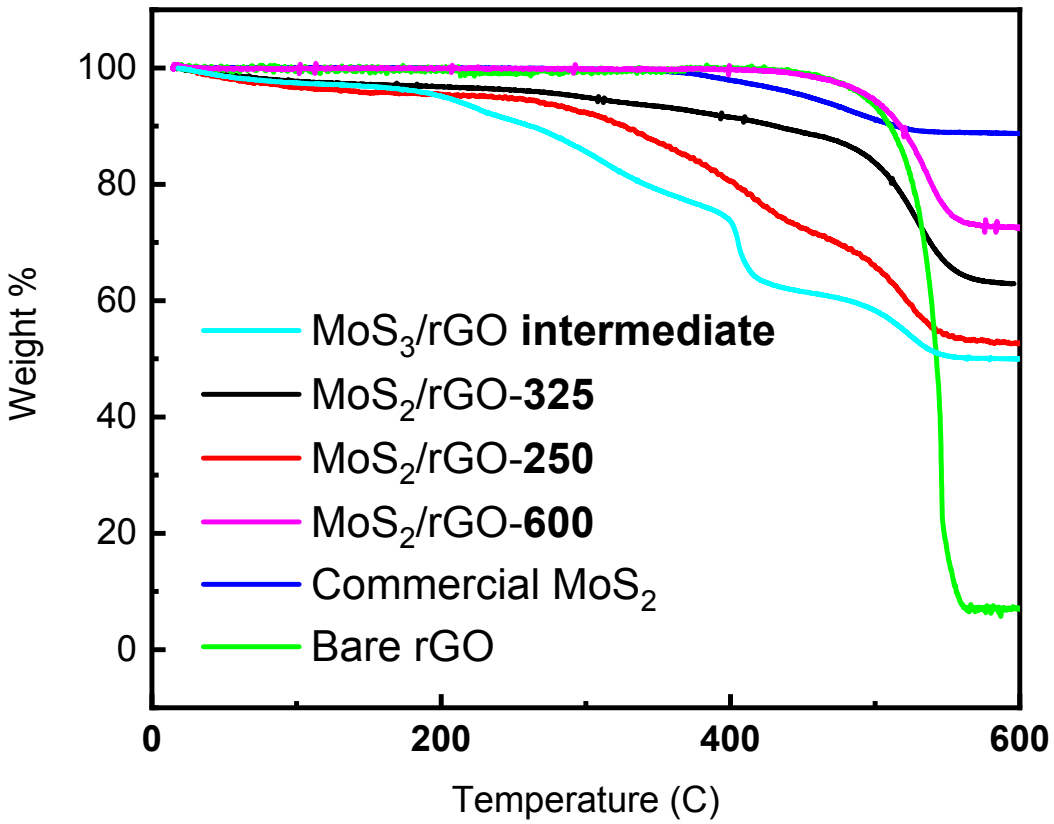

Figure S8. Thermogravimetric analyses of various hybrid materials and control samples (commercial MoS_2 powder and bare rGO synthesized at the same conditions as MoS_2/rGO-600 but without presence of ATM precursors).

Determination of weight % of MoS_2 in MoS_2/rGO-600:

1. Bulk MoS_2 shows gradual weight loss of 10.1% from 370 °C to 600°C due to the conversion of MoS_2 to MoO_3.
2. Control rGO shows a steep weight loss of 93.36% at 420 °C due to the conversion of rGO to graphitic carbon.
3. Based on the above-mentioned weight loss of control samples
4. Weight loss from 370 °C till 600 °C = Weight loss of MoS_2+Weight loss of rGO
   = (Weight% of MoS_2) *10.1% +(1-Weight% of MoS_2) *93.36%
5. Weight% of rGO = 1-Weight% of MoS_2
6. (99.91% - 72.57%) = (Weight % of MoS_2) *10.1% + (1 - Weight % of MoS_2) *93.36%
7. Weight % of MoS_2 in MoS_2/rGO-600 = 79.29%

Table S3: Elemental Analysis of MoS_x/rGO samples

Samples	wt% of N	wt% of C	wt% of H	wt% of O	wt% of S	wt% of Mo[a]	wt% of MoS_x[b]	wt% of rGO[c]	at% of Mo[d]	at% of S[d]	Mo:S[e]
MoS_2/rGO-600	0.30	19.98	0.15	1.17	33.52	44.88	78.40	21.15	13.51	30.69	1:2.3
MoS_2/rGO-325	0.62	22.46	0.31	4.62	31.17	40.82	71.99	27.08	9.58	21.60	1:2.3
MoS_2/rGO-250	1.07	18.62	0.31	5.14	38.56	36.30	74.86	23.76	9.90	31.25	1:3.2
MoS_3/rGO-intermediate	1.82	20.31	0.99	11.07	35.38	30.43	65.81	31.38	6.50	22.36	1:3.4

Note:

Elements: N - Nitrogen; C - Carbon; H - Hydrogen; O - Oxygen; S - Sulfur; Mo - Molybdenum.

[a] Weight percentage of Mo = 100 % - (wt% of C + wt% of N + wt% of H + wt% of O + wt% of S)

[b] Weight percentage of MoS_x = wt% of Mo + wt% of S

[c] Weight percentage of rGO = wt% of C + wt% of O

[d] at% of x = $\frac{\text{wt\% of x/AW of } X}{\sum_{i}^{n}(\text{wt\% of i /AW of i})}$, $AW = atomic\ weight$

[e] Atomic ratio of Mo:S = $\frac{\text{at\% of Mo}}{\text{at\% of S}}$

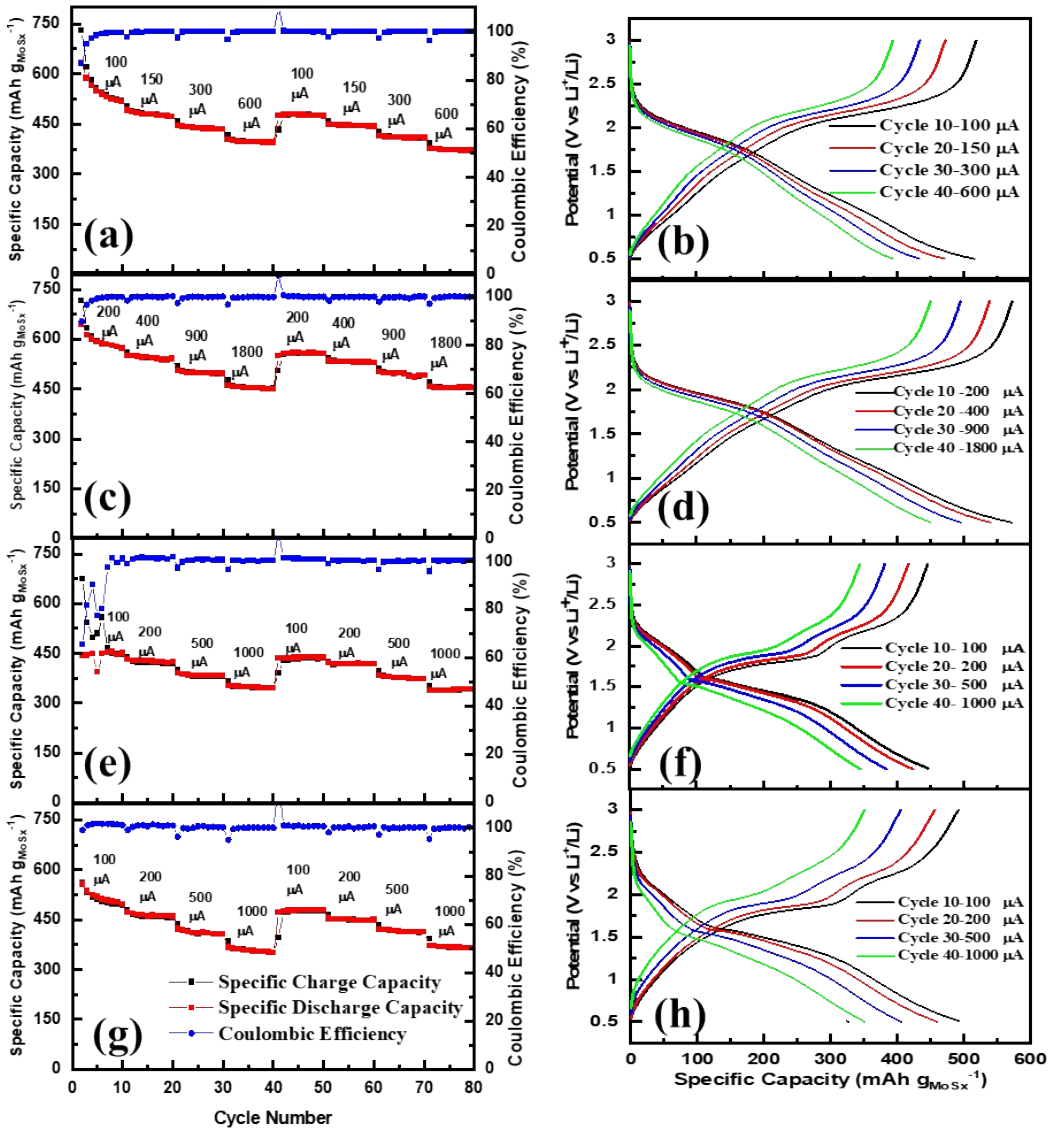

Figure S9. Rate Performance at varied current rates and representative galvanostatic charge/discharge curves of Li-ion half cells with the cathode made of (a, b) MoS_2/rGO-600 (0.88 mg), (c, d) MoS_2/rGO-325 (1.44 mg), (e, f) MoS_2/rGO-250 (0.82 mg) and (g, h) MoS_3/rGO intermediate material (1.76 mg). Panels (a), (c) and (e) have the same legend as panel (g).

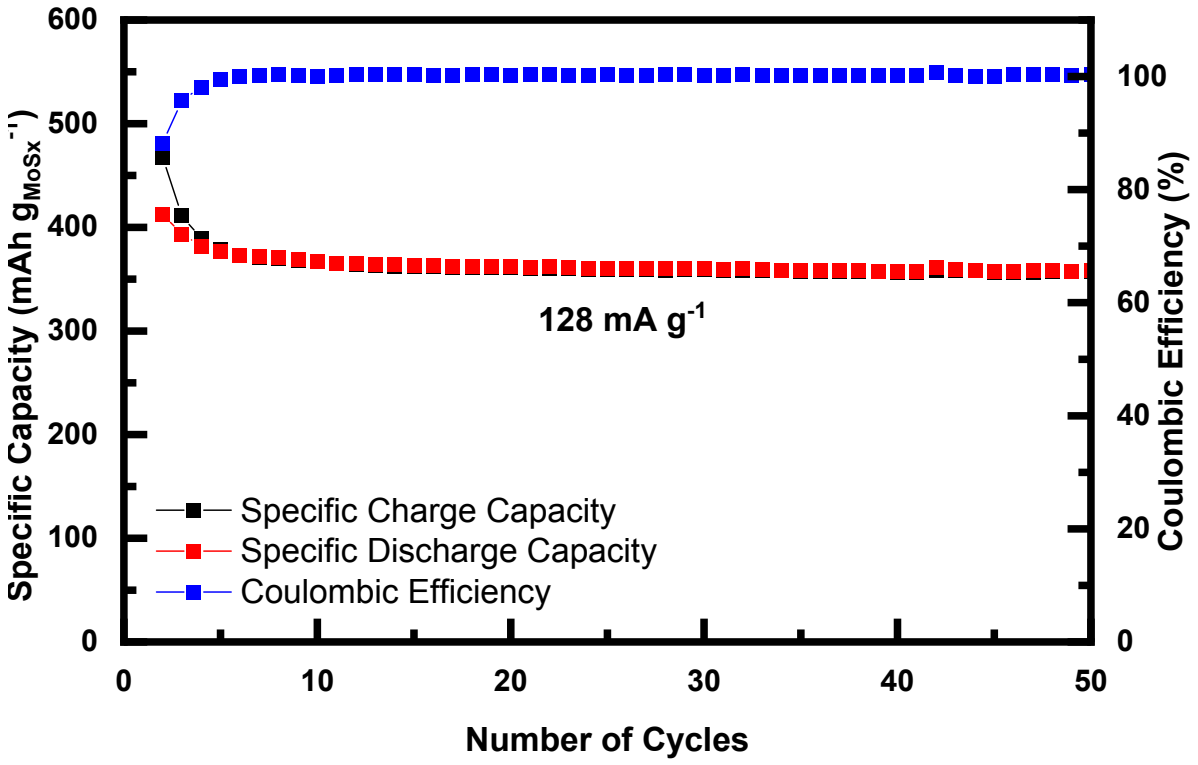

Figure S 10. Long term stability test of Li ion half cells with anode made of MoS_2/rGO-600.

Calculation of the Coulombic efficiency of battery tests:

$$Coulombic\ Efficiency\ of\ MoSx\ in\ LIB = \frac{Specific\ Disharge\ Capacity}{Specific\ Charge\ Capacity} * 100 \quad \rightarrow \textbf{(1)}$$

Calculation of the specific capacity of MoS_x/rGO samples in battery tests:

$$Specific\ capacity\ of\ MoSx = \frac{measured\ capacity}{Total\ Mass\ of\ hybrid\ x\ (wt\%\ of\ MoSx)} \quad \rightarrow \textbf{(2)}$$

Discussion on rGO contribution to the Li-ion storage capacity:

The small contribution from rGO can be deducted from the specific capacity. As shown in Table S3, the stabilized specific capacity at 100 μA charge/discharge current is about 73, 86, 111 and 53 mAh g_{rGO}^{-1} for the corresponding control samples rGO-600, rGO-325, rGO-250 and rGO-intermediate. After deducting these contributions based on the wt% of rGO by equations below Table S3, the specific capacity attributed to MoS_x is adjusted to 499, 540, 411 and 467 mAh g_{MoSx}^{-1} for MoS_2/rGO-600, MoS_2/rGO-325, MoS_2/rGO-250 and MoS_3/rGO-intermediate, respectively. The contribution by rGO is only 3.9%, 5.7%, 8.0% and 5.1% in MoS_2/rGO-600, MoS_2/rGO-325, MoS_2/rGO-250 and MoS_3/rGO-intermediate, respectively. These small corrections are insignificant to the conclusions in the main manuscript.

Table S4. Estimation of contribution to the specific capacity by rGO and MoS_x in LIB

Sample	Specific Capacity of MoSx (mAh/g_{MoSx})[a]	Specific Capacity of rGO (mAh/g_{rGO})[b]	$(wt\% \ of \ rGO / wt\% \ of \ MoSx)$[c]	Corrected Specific Capacity[d] (mAh/g_{MoSx})	Relative Contribution of rGO[e]
MoS_2/rGO-600	519	73	0.27	499	3.9
MoS_2/rGO-325	573	86	0.38	540	5.7
MoS_2/rGO-250	446	111	0.32	411	8.0
MoS_3/rGO-intermediate	492	53	0.48	467	5.1

Note:

[a] Based on the 10th cycle at 100 mA in Figure S8.

[b] Based on the 10th cycle at 100 mA in Figure S10.

[c] Based on the values from Table S2.

[d] Corrected specific capacity = (Specific capacity of MoS_x) - [(Specific capacity of rGO) * ($\frac{wt\%\ of\ rGO}{wt\%\ of\ MoS\ x}$)]

[e] Relative contribution of rGO = $\frac{\text{Specific Capacity of MoSx} - \text{Corrected Specific capacity}}{\text{Specific Capacity of MoSx}} * 100$

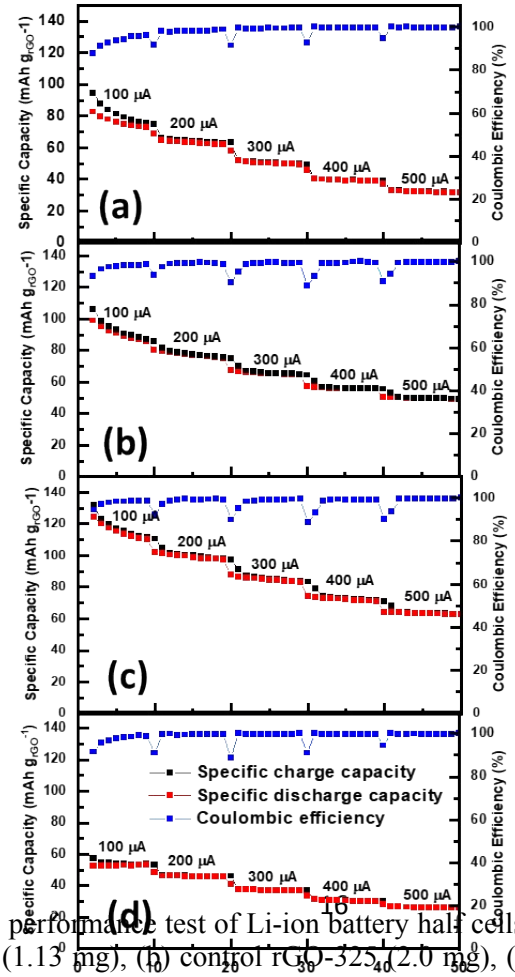

Figure S11. Rate performance test of Li-ion battery half cells with the cathode made of (a) control rGO-600 (1.13 mg), (b) control rGO-325 (2.0 mg), (c) control rGO-250 (1.03 mg) and (d) control rGO-intermediate (1.25 mg). Panels (a), (b) and (c) follow the same legend as panel (d).

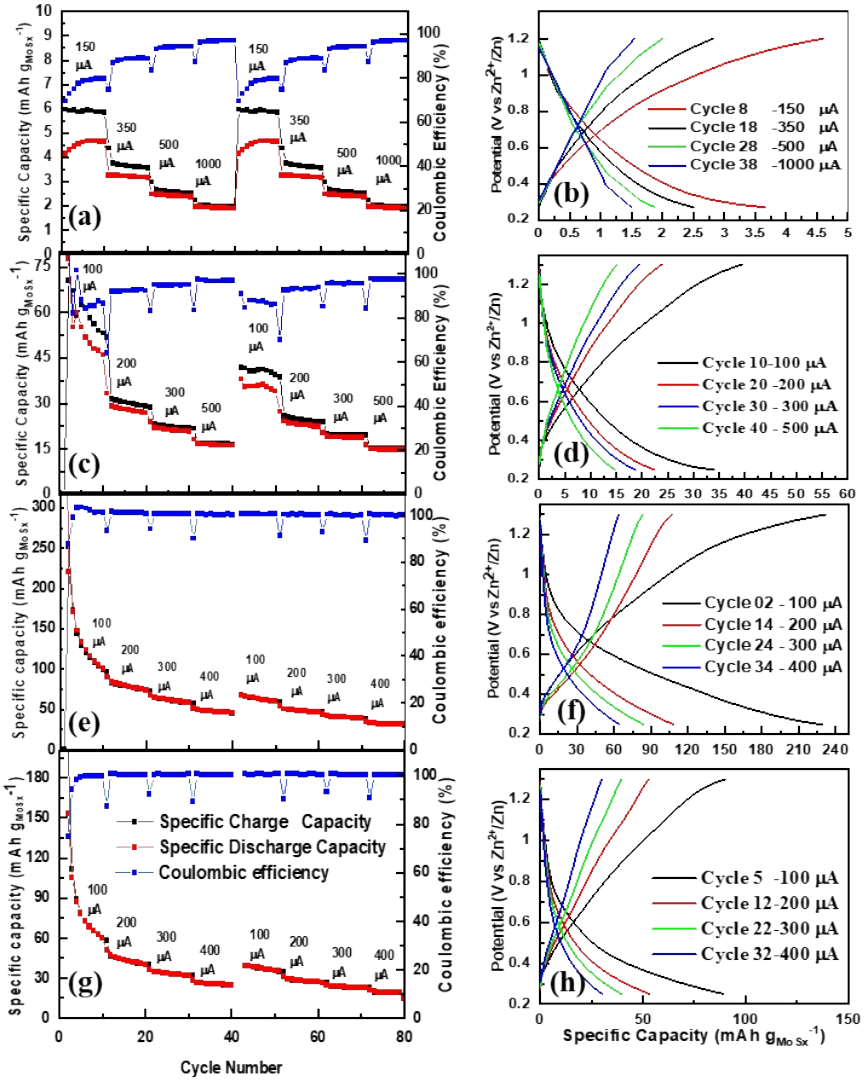

Figure S12. Galvanostatic charge-discharge curves and the rate performance of Zn-ion battery half-cells with the cathode made of (a, b) MoS_2/rGO-600 (0.87 mg), (c, d) MoS_2/rGO-325 (1.36 mg), (e, f) MoS_2/rGO-250(1.28 mg), and (g, h) MoS_3/rGO intermediate hybrid material (0.88 mg). Panels (a), (c) and (e) follow same legend as panel (g).

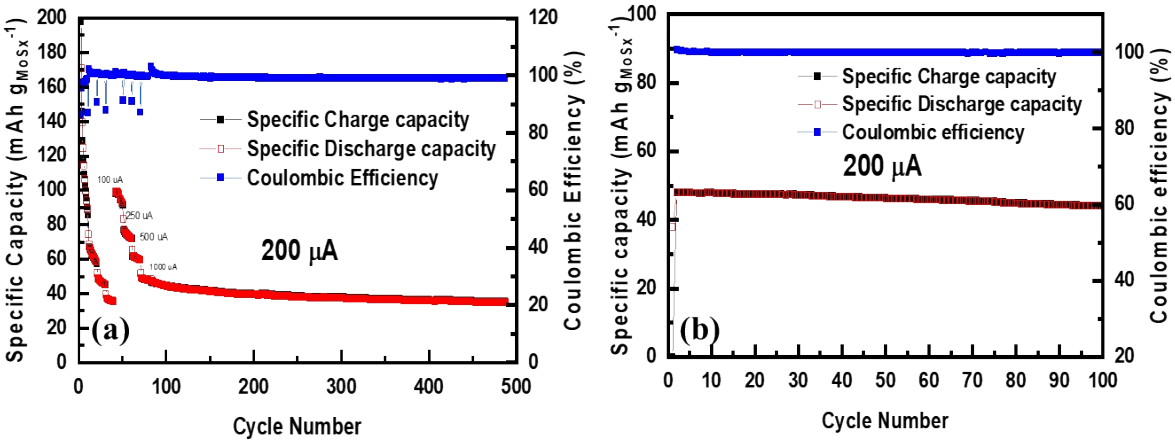

Figure S13. The cycle stability test of Zn-ion battery half-cells with the cathode made of (a) MoS_2/rGO-250 (2.16 mg) and (b) the MoS_3/rGO intermediate material (0.88 mg). The charge/discharge was carried out at 0.25 – 1.30 V vs. Zn^{2+}/Zn.

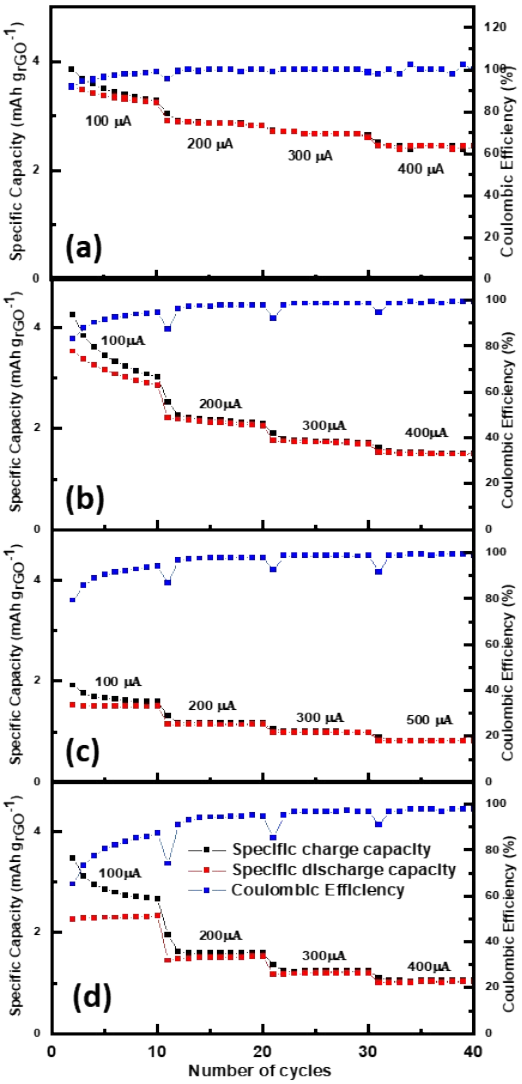

Figure S14. Rate performance test of Zn ion battery half cells with the cathode made of (a) control rGO-600 (1.38 mg) (b) control rGO-325 (2.0 mg) (c) control sample-250 (0.90 mg) (d) control rGO-intermediate (1.50 mg). Panels (a), (b) and (c) follow same legend as panel (d).